Available online at www.sciencedirect.com
SCIENCE DIRECT®
Acta Materialia 52 (2004) 4757–4766
Acta MATERIALIA
www.actamat-journals.com

Solid-state phase transformations involving solute partitioning: modeling and measuring on the level of individual grains

S.E. Offerman [a,b,*], N.H. van Dijk [a], J. Sietsma [b], E.M. Lauridsen [c], L. Margulies [c,d], S. Grigull [d], H.F. Poulsen [c], S. van der Zwaag [e]

[a] Interfaculty Reactor Institute, Delft University of Technology, Mekelweg 15, 2629 JB Delft, The Netherlands
[b] Department of Materials Science and Engineering, Delft University of Technology, Rotterdamseweg 137, 2628 AL Delft, The Netherlands
[c] Center for Fundamental Research: Metal Structures in 4D, Materials Research Department, Risø National Laboratory, 4000 Roskilde, Denmark
[d] European Synchrotron Radiation Facility, BP 220, 38043 Grenoble Cedex, France
[e] Faculty of Aerospace Engineering, Delft University of Technology, Kluijverweg 1, 2629 HS Delft, The Netherlands

Received 20 November 2003; received in revised form 11 June 2004; accepted 16 June 2004
Available online 30 July 2004

Abstract

A simplified grain growth model is presented for the transition from non-overlapping to overlapping diffusion fields of growing neighboring grains during partitioning solid-state transformations in polycrystalline materials. The model is based on unique observations on the austenite decomposition into ferrite and pearlite in medium-carbon steel with the three-dimensional X-ray diffraction microscope. The model explains three types of observed pro-eutectoid ferrite grain growth and austenite grain decomposition, and the indirectly observed carbon exchange between decomposing austenite grains. A direct comparison of the model and the experiment at the level of individual grains shows that the growth of ferrite grains is strongly related to the local carbon concentration and the local density of nuclei. Unusual observations of a non-stationary austenite grain size prior to the transformation, and oscillatory ferrite growth are reported.

Keywords: Ferritic steels; Phase transformation kinetics; X-ray diffraction; Synchrotron radiation; Analytical methods

1. Introduction

The evolution of the microstructure during the formation of polycrystalline materials has been studied extensively worldwide for many decades [1–3]. Understanding the evolution of the microstructure is of technological relevance for the development of new materials with optimal mechanical properties and for improving existing materials and their production process. However, the subject is difficult to study experimentally, because there are a large number of relevant parameters that need to be probed simultaneously, in situ, and in the bulk of the material, in order to obtain a full description of the mechanisms involved. Moreover, ab initio calculations that predict microstructural properties from first principles require at present too much computer time as the problem involves length scales from nanometers up to micrometers and time scales from seconds up to minutes or even hours.

Generally, the modeling of the evolution of the microstructure during the formation of a new phase from the parent phase during phase transformations involving solute partitioning is divided into two parts: grain nucleation and grain growth. During the nucleation stage small stable particles of the new phase are formed in the parent phase due to local fluctuations in structure and composition, as a result of thermal motion, which can be described by the classical nucleation theory [1]. In phase transformations involving solute partitioning the growth stage is characterized by a pile-up or depletion of solute atoms in front of the interface between the parent phase and the new phase. The presence of these diffusion

* Correspondig author. Tel.: +31-15-278-2198; fax: +31-15-278-6730.
E-mail address: S.E.Offerman@tnw.tudelft.nl (S.E. Offerman).

1359-6454/$30.00 © 2004 Acta Materialia Inc. Published by Elsevier Ltd. All rights reserved.
doi:10.1016/j.actamat.2004.06.030

fields naturally leads to a further refinement in the description of the growth in two stages: (a) the early stage of the transformation in which the diffusion fields of growing grains do not overlap and (b) the later stage of the transformation in which the diffusion fields do overlap. The growth ends with the hard impingement of grains.

When introducing the initial microstructure in the models, spheres are the simplest geometrical shapes to represent the grains in polycrystalline materials [4]. This spherical grain concept has indeed been elaborated successfully by Vandermeer [5] for the austenite–ferrite transformation, in which a layer of ferrite that completely covers the former austenite/austenite grain boundary grows towards the interior of the austenite grain. However, when modeling the parent grains as spheres, a logical introduction of well-known specific nucleation sites, such as quadruple points, grain boundary edges, and grain boundary faces, each with their own nucleation characteristics, is not possible. The development of single-grain models [6] has created the possibility to model the parent grain geometry and the phase transformation kinetics in detail, without consuming too much computer time. However, multiple grain effects, such as diffusion of alloying elements between parent grains, are not included. As will be shown in the remainder of the paper, there are now experimental indications that such processes indeed do take place, which need to be taken into account in order to make a quantitative prediction of the evolution of the microstructure.

Recently, a new technique has become available to measure phase transformations (and recrystallization) at the level of individual grains within the bulk of a sample: three-dimensional X-ray diffraction (3DXRD) microscopy [7–9]. The technique gives simultaneous and in situ information about the fractions of the parent phase and the new phase, the number of nuclei of the new phase, the growth of individual new grains, and the decomposition of the parent grains.

In a previous paper, we have shown the experimental observation of the nucleation and growth of individual ferrite grains during slow cooling of medium carbon steel with the 3DXRD-microscope [10]. We showed that four types of ferrite growth could be distinguished. The first type is well described by the classical theory [11] of diffusion-controlled growth during the early stage. However, it was also shown that the growth of the first type deviated from the classical theory at a later stage and that the three other types of grain growth did not conform to theory at any point. In this paper, we extend the classical growth theory with a simplified treatment of overlapping diffusion fields. In addition, we present new experimental observations on the decomposition of individual austenite grains, which gives a more complete picture of the solid-state phase transformations, and in particular the role of the partitioning solute atoms.

2. Grain growth and grain decomposition model

In the following, we present a simplified model for the diffusion-controlled grain growth involving the transition from non-overlapping to overlapping diffusion fields during solid-state transformations. In the model, we will assume a spherical geometry of both the parent and new grains. The early growth stage is then well described by the theory of Zener [11] for diffusion-controlled grain growth. An approximate treatment of the later growth stage was given by Wert and Zener [12] for slightly supersaturated solutions. In this analysis, it was assumed that for slightly supersaturated solutions, the interfaces all move sufficiently slowly for the steady-state solution to be appropriate. This assumption has also been adopted by others [13]. Gilmour and co-workers also developed a model for the later growth stage, but then for the one-dimensional growth of planar grain boundaries, which is also valid for three-dimensional growth in highly supersaturated solutions [14,15]. However, during the process of soft impingement, i.e. the overlap of diffusion fields, the degree of supersaturation generally changes from high when the diffusion fields just overlap, to low when the grains are close to hard impingement. The soft impingement model presented here is independent of the degree of supersaturation.

2.1. Non-overlapping diffusion fields

The first theoretical treatment for the diffusion-controlled growth was given by Zener [11] for a spherical precipitate in a solid solution of initially uniform composition. During the initial stage of the transformation, in which the growth of the individual grain is not limited by interactions with neighboring grains due to overlapping diffusion fields (soft impingement) or existing grain boundaries (hard impingement), the radius of the new grain R_n as a function of time t is given by the Zener model as

$$R_n(t) = \chi\sqrt{\langle D\rangle(t - t_s)}, \tag{1}$$

where $\langle D\rangle$ is the average diffusion coefficient of the solute atoms over the concentration gradient near the interface [5,16] and t_s is the moment of nucleation of the grain. χ can be approximated by [11,17]

$$\chi = 2.102\left(\frac{C^p_\infty - C^p_{eq}}{C^n_{eq} - C^p_\infty}\right)^{0.5871}, \tag{2}$$

where C^n_{eq} and C^p_{eq} are the equilibrium concentration of the solute atoms in the new and parent phase, respectively, and C^p_∞ is the concentration of solute atoms in the

parent phase far away from the interface, which is equal to the initial concentration C_0 of solute atoms during the initial stage of the transformation. Eqs. (1) and (2) where derived under the following assumptions:

1. The concentration of the solute atoms at either side of the interface corresponds to the equilibrium values, given by the phase diagram.
2. The rate of growth is solely limited by diffusion (the lattice transformation is much faster than the redistribution of solute atoms).
3. The rate of advance of the interface is related to the gradient of the carbon concentration at the interface.
4. The diffusion of the solute element in the new phase is so fast that the solute concentration gradient in the new phase is zero.
5. Only the diffusion of one solute element is considered.

During continuous cooling the grain radius needs to be calculated for each time step by determining the velocity of the interface from Eq. (1), because both the diffusion coefficient and the equilibrium concentration of solute atoms in the parent phase depend on temperature [17].

2.2. Overlapping diffusion fields

As the transformation proceeds, the diffusion fields of neighboring grains start to overlap, which slows down the growth rate of the grains of the new phase. This process is referred to as soft impingement. Generally, the process of soft impingement can be subdivided into two stages. During the early stage of soft impingement, the diffusion fields only overlap in a limited number of directions, which results in different gradients in solute concentration in different directions around the grain under consideration. The later stage of soft impingement is characterized by a diffusion field that is approximately the same in all directions around the grain under consideration. The reason for this is that soft impingement has taken place in all directions at this stage and that the diffusion fields between the different neighboring grains also overlap.

An exact analytical description of the first stage of soft impingement will be complex, because the different gradients in solute concentration in different directions around the grain under consideration make the problem asymmetric. However, in the case that the nucleation density is large and the diffusion of the solute atoms is fast, the early stage of soft impingement is short. In the following description of soft impingement, the early stage of soft impingement is therefore neglected. It is assumed that the diffusion field surrounding the grain under consideration is the same in all directions as soon as the moment at which soft impingement first occurs in an averaging approach. As a first approximation, the later stage of soft impingement can be described by the overlap of the diffusion field of the grain under consideration and the diffusion field of an average spherical ferrite grain (with an average size at an average distance) along the direction of the centres of the two spheres.

In this approximate treatment of the later stage of soft impingement, the Zener theory can still be used, but the concentration C^{p}_{∞} of solute atoms in the parent phase far away from the interface is not equal to the overall concentration of solute atoms anymore. The concentration of solute atoms in the parent phase far away from the interface is now equal to the concentration of the solute atoms where the diffusion fields of neighboring grains intersect. In this section, an expression is derived for the concentration of the solute atoms where the diffusion fields of neighboring grains intersect. The moment at which the diffusion field of an individual grain starts to overlap with those of neighboring grains depends on the local density of nuclei, the average growth rate of the neighboring grains, and the concentration profiles of the solute atoms in front of the advancing interfaces. The average distance between the centers of neighboring nuclei $\langle d\rangle$ is estimated from the average volume in which one spherical grain can grow before hard impingement takes place for a given local density of nuclei $N^{\mathrm{n}}_{\mathrm{loc}}$ of the new phase. This criterion is expressed by

$$\frac{4}{3}\pi\left(\frac{\langle d\rangle}{2}\right)^3 = \frac{1}{N^{\mathrm{n}}_{\mathrm{loc}}}. \tag{3}$$

The volume of an average grain of the new phase during the transformation can be approximated by

$$\frac{4}{3}\pi\langle R_{\mathrm{n}}\rangle^3 = \frac{f_{\mathrm{n}}}{N^{\mathrm{n}}_{\mathrm{loc}}}, \tag{4}$$

where $\langle R_{\mathrm{n}}\rangle$ is the radius of the average grain and f_{n} is the fraction of new phase at a certain stage of the transformation.

Instead of using Zener's exact solution of the concentration profile, a simplified treatment is adopted in order to find analytical expressions for the effect of overlapping diffusion fields on the grain growth. The length of the diffusion field L_{i} of an individual grain can be determined by assuming a linear concentration profile of the solute atoms in front of the interface, see Fig. 1. The concentration $C^{\mathrm{p}}_{\mathrm{i}}$ of solute atoms in front of the interface of an individual spherical grain under consideration can then be written as

$$C^{\mathrm{p}}_{\mathrm{i}}(r) = C^{\mathrm{p}}_{\mathrm{eq}} - (C^{\mathrm{p}}_{\mathrm{eq}} - C_0)\frac{r - R_{\mathrm{n}}}{L_{\mathrm{i}}}, \tag{5}$$

in the region where $R_{\mathrm{n}} \leqslant r \leqslant R_{\mathrm{n}} + L_{\mathrm{i}}$.

The present linear approximation of the diffusion field differs from the linear approximation as given by Zener [11]. The latter approximation is limited to concentration profiles that form a thin shell surrounding the spherical particle, which is the case for highly supersaturated solutions, i.e. $|C^{\mathrm{n}}_{\mathrm{eq}} - C^{\mathrm{p}}_{\infty}| \ll |C^{\mathrm{n}}_{\mathrm{eq}} - C^{\mathrm{p}}_{\mathrm{eq}}|$.

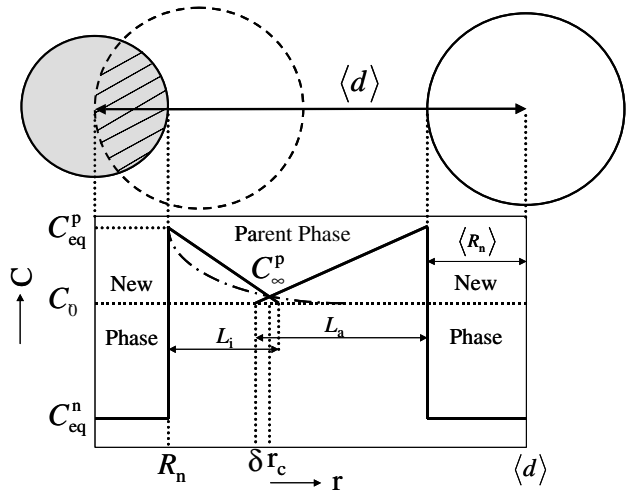

Fig. 1. Model for solid-state phase transformations in polycrystalline materials involving solute partitioning. The gray area represents the calculated grain volume of the new grain. The hatched area represents the overlap volume of the new grain and parent grain, which is equal to the decrease in parent grain size. The concentration C of the diffusing element is shown along the radial coordinate r from the center of the new grain to the center of the average neighboring grain. The segmented line represents the exact concentration profile of the diffusion element in front of the interface in the parent phase, which is approximated by a linear concentration profile (solid lines). The other symbols are explained in the text.

The present linear approximation is independent of the degree of supersaturation. The length L_i is then found by considering the mass balance of solute atoms that have moved from the new phase to the parent phase. This mass balance can be written as

$$\int_0^{R_n}\left(C_0 - C^{n}_{eq}\right)4\pi r^2\,dr = \int_{R_n}^{R_n+L_i}\left(C^{p}_{i}(r) - C_0\right)4\pi r^2\,dr. \tag{6}$$

Substitution of Eq. (5) in Eq. (6), integrating and rearranging gives

$$L_i^3 + 4R_nL_i^2 + 6R_n^2L_i - 4R_n^3B = 0 \tag{7}$$

with

$$B = \frac{C_0 - C^{n}_{eq}}{C^{p}_{eq} - C_0}. \tag{8}$$

Solving Eq. (7) with respect to L_i gives

$$L_i = \left\{\frac{1}{3}\left(44 + 54B + 6\sqrt{54 + 132B + 81B^2}\right)^{1/3} - \frac{2}{3\left(44 + 54B + 6\sqrt{54 + 132B + 81B^2}\right)^{1/3}} - \frac{3}{4}\right\}R_n. \tag{9}$$

The concentration C^{p}_{a} of solute atoms in front of the interface of the spherical, average neighboring grain in the region where $\delta \leqslant r \leqslant \delta + L_a$ can be written as

$$C^{p}_{a}(r) = C_0 + (C^{p}_{eq} - C_0)\frac{r-\delta}{L_a}, \tag{10}$$

where L_a is the length of the diffusion field that corresponds to the radius of the average spherical grain of the new phase. δ is the distance from the center of an individual nucleus to the end of the diffusion field of the average neighboring grain, given by

$$\delta = \langle d\rangle - \langle R_n\rangle - L_a = \sqrt[3]{\frac{3}{4\pi N^{n}_{loc}}}\left(2 - \sqrt[3]{f_n}\right) - L_a. \tag{11}$$

The length L_a of the diffusion field that corresponds to the average grain radius of the new phase can be determined by substituting $R_n = \langle R_n\rangle$ into Eq. (9).

The position r_c at which the linear diffusion profiles of the grain under consideration and the average neighboring grain intersect can then be found by equating Eqs. (5) and (10). Rearranging gives

$$r_c = \frac{L_a(R_n + L_i) + L_i\delta}{L_a + L_i}. \tag{12}$$

The concentration C^{p}_{c} of the solute atoms at the position where the linear diffusion profiles intersect is then given by

$$C^{p}_{c} = C^{p}_{i}(r_c) + C^{p}_{a}(r_c) - C_0 = C_0 + \left(C^{p}_{eq} - C_0\right)\frac{(R_n + L_i)(L_a + L_i) - L_a(R_n + L_i) - L_i\delta}{L_i(La + L_i)}. \tag{13}$$

The two stages of grain growth can now be described with the theory of Zener by changing the concentration C^{p}_{∞} of solute atoms in the parent phase far away from the interface. In the case that $R_n + L_i \leqslant \delta$, the grain radius of the new grain is given by Eqs. (1) and (2) with $C^{p}_{\infty} = C_0$. In the case that $R_n + L_i > \delta$, the grain radius of the new grain is also given by Eqs. (1) and (2), but with $C^{p}_{\infty} = C^{p}_{c}$.

2.3. Parent grain decomposition

The growth of grains of the new phase is accompanied by a decrease in grain size of the parent grains. In the present model, we assume that the transformation starts with the formation of a nucleus of the new phase on the grain boundary of a spherical parent grain. The volume $V_{p\to n}$ of the parent grain that is replaced by the new grain (see Fig. 1) is then given by

$$V_{p\to n} = \frac{4\pi}{3}\left(\frac{1}{2} - \frac{3}{16}\frac{R_n}{R_{p,0}}\right)R_n^3, \tag{14}$$

where R_n is the radius of the new grain and $R_{p,0}$ is the original parent-grain radius before the transformation. The volume of the parent grain V_p for a given degree of overlap can then be calculated from

$$V_p = V_{p,0} - V_{p\to n}, \tag{15}$$

where $V_{p,0}$ is the original parent grain volume before the transformation.

3. Experimental

The material used is hot-rolled C–Mn steel (0.214 wt% C, 0.513 wt% Mn, 0.200 wt% Si) with a regular initial ferrite–pearlite microstructure. The steel is covered with a thin coating of nickel and positioned in a furnace with a helium flow in order to prevent decarburization. The steel is austenitized at 900 °C for 10 min, and subsequently continuously cooled to 600 °C in 1 h, i.e. at a cooling rate of 5 °C/min. This experiment is then repeated once more on the same steel sample.

In order to study the time evolution of individual grains during phase transformations, a relatively small volume of steel is illuminated with a monochromatic beam of hard (penetrating) X-rays from a synchrotron source. For the experiment described here, we used the 3DXRD microscope at beam line ID11 of the European Synchrotron Radiation Facility in transmission geometry. The energy of the monochromatic X-rays is 80 keV (wavelength of 1.55×10^{-2} nm). The beam size is 94×97 μm^2, and the thickness of the sample is 400 μm. By slightly rotating the sample around an axis perpendicular to the beam, over an angle of 1.6°, a number of grains give rise to diffraction spots on a 2D-detector. Fig. 2 shows a diffraction pattern halfway through the austenite to ferrite transformation.

From the standard diffraction theory, it can be shown that the intensity of each spot is proportional to the volume of the grain it originates from [18]. The intensity of the spot that originates from an individual ferrite grain is normalized with respect to the total intensity of the same ferrite diffraction ring at the end of the transformation, by assuming that the equilibrium ferrite fraction is then reached [19]. In an analogous manner, an expression is found for the volume of individual austenite grains. The intensity of a single austenite grain is normalized to the powder intensity of the austenite before the start of the transformation.

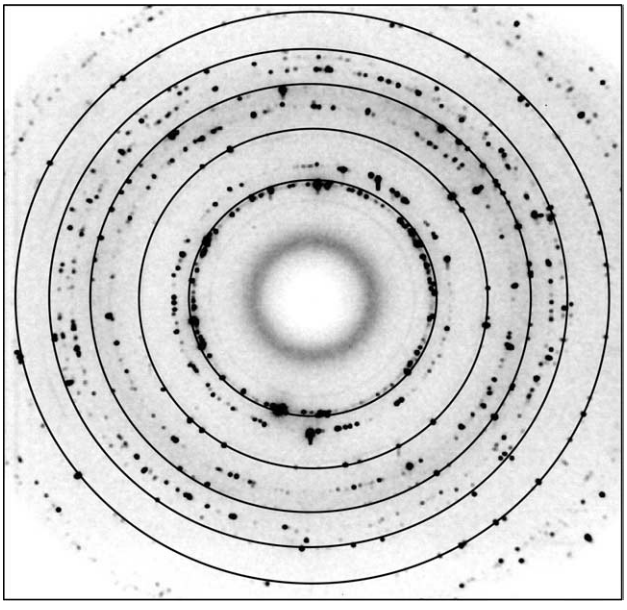

Fig. 2. X-ray diffraction pattern of the steel showing austenite and ferrite (on solid rings) reflections at 763 °C, which is approximately half way the transformation.

Given the experimental conditions the radius of the smallest detectable austenite grain is about 2 μm. Once every six exposures the beam size is expanded to 139×139 μm^2 in order to check whether the total volume of the grain is illuminated by the small central beam. In order to check if the total integrated intensity from a single grain is obtained by rotating the sample from −0.8° to 0.8°, we took additional exposures for rotation angles from −2.4° to −0.8° and from 0.8° to 2.4°. In the present experiment the transformation is studied with a typical time resolution of 10 s.

The fraction of the new phase is obtained by averaging the intensities of the three rotation-scans of a powder ring that were measured each time the beam size was extended to 139×139 μm^2. This average intensity $\langle I\rangle$ was then normalized to the intensity at the end of the transformation $\langle I\rangle_f$ and multiplied by the final fraction at the end of the transformation that is calculated with MTDATA®, leading to: $f^n = \left(\langle I\rangle/\langle I\rangle_f\right) f_f^n$. In an analogous manner the fraction of the parent phase is obtained, but then by normalizing to the powder intensity before the transformation.

4. Experimental results

4.1. Ferrite and austenite fractions

Fig. 3 shows the measured ferrite (f^α) and austenite (f^γ) volume fractions as a function of temperature compared to the equilibrium fractions as calculated from the thermodynamic database MTDATA®. The calculated transition temperature from austenite to ferrite is $A_3 = 826$ °C and the temperature range of the transition from austenite to cementite is between $A_1^+ = 718$ °C and $A_1^- = 711$ °C, respectively. The final ferrite fraction at the end of the transformation as calculated with MTDATA® is $f_f^\alpha = 0.98$, which includes the pearlitic ferrite. Each experimental ferrite fraction in Fig. 3 is the average of the ferrite fractions obtained from the {2 0 0} and {2 1 1} powder rings for the two continuous-cooling measurements. In an analogous manner the austenite fractions of Fig. 3 are determined from the {2 0 0} and {2 2 0} reflections of the austenite powder rings.

Fig. 3 shows that the ferrite and austenite fractions change approximately according to thermodynamic

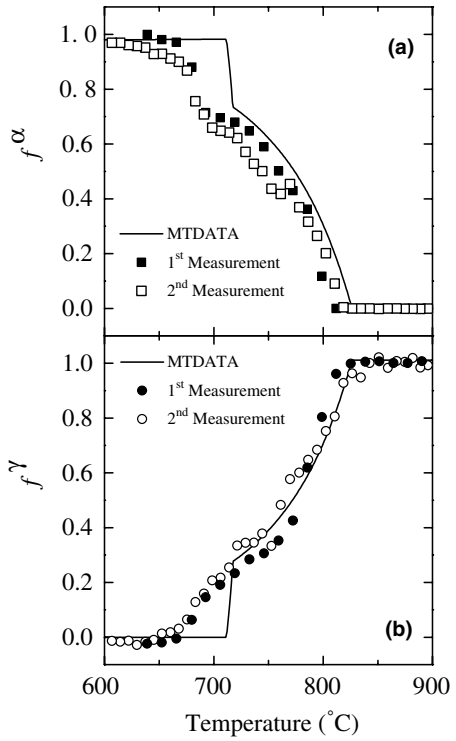

Fig. 3. The measured ferrite f^{α} (a) and austenite f^{γ} (b) volume fractions as determined from the intensity of the powder diffraction rings for two experiments compared to the equilibrium fractions as determined from the thermodynamic database MTDATA® (solid lines). The error in the counting statistics is smaller than the symbol size.

equilibrium during the austenite to ferrite phase transformation. Fig. 3(a) shows that the ferrite formation starts at 822 °C, which is only slightly lower than the thermodynamic equilibrium transformation temperature. The pearlite formation starts at 685 °C, which is 33 °C lower than the thermodynamic equilibrium transition temperature (A_1^+) that was calculated from MTDATA®. This is caused by the relatively high energy barrier for the nucleation of pearlitic cementite during the formation of pearlite [20] compared to the activation energy for nucleation of pro-eutectoid ferrite [10].

The difference in fraction between the two measurements results from the relatively small beam size and $\Delta\omega$-range that was used to obtain a powder average. The small difference between the starting temperature for the increase of the ferrite fraction and the decrease of the austenite fraction is the result of the relatively small number of ferrite grains and the large number of austenite grains that are present at the start of the transformation, which decreases the signal to noise ratio. Moreover, a comparison of the integrated intensity of the different powder rings showed the absence of significant texture.

4.2. Nucleation of ferrite

The number of ferrite nuclei as a function of temperature is obtained by counting the number of ferrite spots on the detector during the transformation. Fig. 4 shows the measured overall number of ferrite nuclei $N^{\alpha}_{\mathrm{norm}}$ that is normalized to the maximum number of nuclei, as a function of temperature. Due to the small rotation of the sample only a limited, but representative number of ferrite nuclei could be measured. The nucleation behavior is described in more detail in [10], but will be used here as an input parameter for the model described in Section 2.

4.3. Growth of ferrite grains

Four types of ferrite growth were experimentally observed [10], and are shown in Fig. 5, which gives the

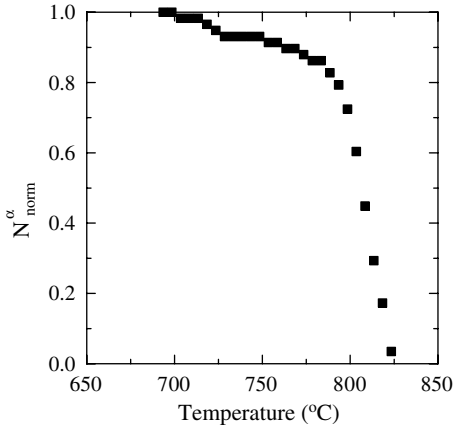

Fig. 4. The measured, overall density of ferrite nuclei that is normalized to the maximum value.

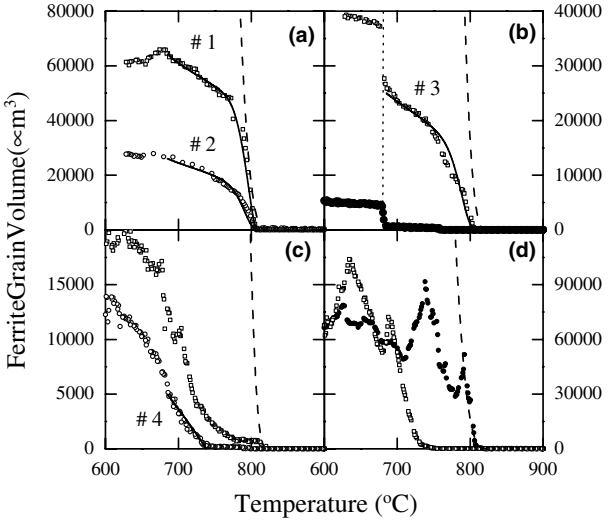

Fig. 5. Measured and modeled volume of individual ferrite grains as a function of temperature. Ferrite growth in involving the transition from non-overlapping to overlapping diffusion fields with neighboring grains (a), ferrite continues to grow into pearlite (b), retarded ferrite (c) growth, and (d) oscillatory ferrite growth. The error in the counting statistics is smaller than the symbol size.

volume of a number of individual ferrite grains during growth. The first and most frequently observed type of ferrite grain growth is shown in Fig. 5(a). The grain with the largest final grain volume in Fig. 5(a) clearly shows two growth stages, which is in agreement with the model described in Section 2. The early growth stage is faster than the later growth stage, corresponding to the transition from non-overlapping to overlapping diffusion fields during the progress of the transformation. The smaller grain in Fig. 5(a) does not show the two different growth stages so clearly, indicating that the diffusion fields overlap at an early stage. At the temperature at which the pearlite forms (685 °C), the ferrite growth is already completed or proceeds at an unchanged rate until the final size is obtained. For these grains, pearlite formation elsewhere in the structure did not affect their growth.

Fig. 5(b) shows a second type of growth: in which the ferrite grain continues to grow as part of a pearlite colony. Initially, the ferrite growth resembles that of the grains shown in Fig. 5(a): a rapid initial growth followed by a slower growth stage due to overlapping diffusion fields. However, at the temperature of 685 °C (indicated by the thin dashed line) the grains all show a rapid increase in grain volume. As each diffraction spot corresponds to the ferrite lattice being in a particular orientation in space, the rapid increase of the diffraction spot intensity at the pearlite temperature must mean that these pro-eutectoid ferrite grains continue to grow as the lamellar ferrite in a pearlite colony, without a change in crystallographic orientation. Although earlier optical microscopy measurements with polarized light [2] and transmission electron microscopy measurements [21] have already shown that a transition of pro-eutectoid ferrite growth into lamellar ferrite growth is possible, the current measurements are the first 3D and in situ observation of this phenomenon. This mechanism of continued growth of pre-existing ferrite appears to be the dominant mechanism for pearlite formation for the conditions imposed here, as very few new pearlitic ferrite nuclei were found in the pearlite formation temperature range (see Fig. 4). The ferrite growth curves in Fig. 5(b) also show that the ratio of the pro-eutectoid ferrite to the ferrite-in-pearlite volume is not equal for each grain. Based on limited statistics, the pearlite colony seems to reach a larger final size relative to the ferrite grain that it has grown from, when the initially formed ferrite grain is smaller.

Fig. 5(c) shows examples of ferrite growth that is so much retarded that the initial fast growth stage is not present. The diffusion field of these grains overlaps with that of the surrounding grains soon after the particle nucleated.

Finally, a totally unexpected form of ferrite growth is shown in Fig. 5(d). In this least frequently observed growth mode, ferrite grains not only grow, but also shrink temporarily upon continued cooling. This behavior is provisionally attributed to a complex ferrite–ferrite interaction. The neighboring ferrite grains are assumed to make direct contact, but their grain boundaries are not yet in their equilibrium position. Grain boundary tension then causes the ferrite grains to change shape and some of them to shrink. At the same time the transformation continues, which can lead again to growth.

4.4. Decomposition of austenite grains

The formation of the ferrite grains is necessarily accompanied by a decrease in size and finally a disappearance of the austenite grains. Hence, information on the ferrite formation can also be found by analyzing the intensity of specific austenite diffraction spots. We searched typically 50 austenite spots in the diffraction pattern to find decomposition behavior of individual austenite grains that resemble the four ferrite growth modes presented in Fig. 5(a)–(d). The results are shown in Fig. 6 for the modes of Fig. 5(a)–(c), respectively. It should be stressed that the current data set does not contain accompanying pairs of austenite and ferrite grains as in the experimental set-up used it is not possible to link the growing ferrite grain unambiguously to the particular austenite grain in which it was formed.

Fig. 6(a) shows the decrease in austenite size resulting from the growth of a ferrite grain that nucleated in a region with a relatively low local carbon concentration

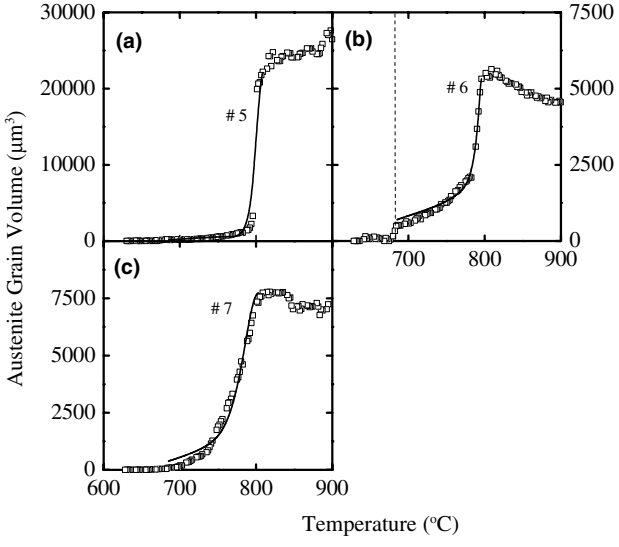

Fig. 6. Measured and modeled volume of individual austenite grains as a function of temperature. The decrease in austenite size corresponds to the first three types of ferrite growth: Ferrite growth in involving the transition from non-overlapping to overlapping diffusion fields with neighboring grains (a), ferrite continues to grow into pearlite (b), and retarded ferrite (c) growth. The error in the counting statistics is smaller than the symbol size.

and a low local density of nuclei. The ferrite grain could largely consume the austenite grain before its diffusion field started to interfere with neighboring diffusion fields. Note that the austenite volume decreases continuously to zero with decreasing temperature, without a detectable change in rate of decrease at the onset of the pearlite formation temperature. From this, we deduce that this austenite grain transformed completely into ferrite and no pearlite formed. The rate of decrease in austenite grain volume does not display abrupt changes, which would have been indicative of the formation of a second or third ferrite grain growing into this austenite grain. It therefore follows that the austenite grain transformed completely into one ferrite grain. The formation of just one ferrite grain per austenite grain for the steel composition and thermal conditions imposed is in good agreement with the findings of Millitzer et al. [22].

For the austenite grain shown in Fig. 6(a) no indications were observed of pearlite formation, suggesting that most of the carbon originally present in the austenite grain must have diffused into neighboring austenite grains. This is only possible if the ferrite formation did not occur around the entire grain boundary of this particular grain, which is in line with the assumed formation of only one ferrite grain in this austenite grain. Of course such a 'carbon leak' also requires that the neighboring austenite grain does not have a growing ferrite grain present at the joint boundary. The carbon repulsion into neighboring grains is of course known to occur for slow cooling rates and is an important phenomenon in band formation [23]. An interesting observation from Fig. 6(a) is the decrease in austenite grain volume prior to the onset of the transformation. The observation indicates that austenite grains still change in volume during the final stages of annealing at a temperature of 900 °C, likely due to coarsening effects.

Fig. 6(b) shows an austenite grain transforming partly into pro-eutectoid ferrite and partly into pearlite. Fig. 6(b) clearly shows the two growth stages of the pro-eutectoid ferrite grain. Moreover, there is perfect agreement in the onset temperature for pearlite formation in Figs. 5(b) and 6(b). Since the average carbon concentration of the steel is 0.214 wt%, approximately one quarter of the original austenite grain volume is expected to transform into pearlite, if no carbon would leak to neighboring austenite grains. While an analysis of the temperature dependence of the integrated intensities of all diffraction spots on a particular austenite diffraction ring confirms such an average pearlite fraction (see Fig. 3), for this particular grain the volume fraction of austenite that is transformed into pearlite is distinctly smaller. For this curve again, a change (in this case an increase) in the austenite grain volume prior to the transformation was observed.

Fig. 6(c) shows an austenite grain that is consumed by a ferrite grain that presumably nucleated in a region with a relatively high initial carbon concentration and a high local density of nuclei. Therefore, the diffusion field of the ferrite grain almost immediately starts to interfere with diffusion fields from neighboring grains. As in the curve of Fig. 6(a), no signs of pearlite formation was found for this austenite grain showing the delayed transformation behavior. For this particular curve the austenite volume prior to the transformation remained relatively constant.

Finally, we did not observe an accompanying image of the fourth type of ferrite grain growth, the oscillatory growth behavior (see Fig. 5(d)) in any of the about 50 austenite grains analyzed. Such an absence of this oscillatory behavior would support our earlier hypothesis that the complex ferrite grain growth, as shown in Fig. 5(d), is the result of a direct interaction between ferrite grains rather than a reversed transformation into austenite.

5. Comparison of theory and experiment

The volume of individual ferrite and austenite grains as a function of temperature is fitted to the model presented in Section 2 of this paper, by assuming para-equilibrium conditions. Para-equilibrium means that the substitutional alloying elements are unable to partition during the time-scale of the experiment, although carbon, which is a fast diffusion interstitial element, redistributes between the austenite and ferrite phases and reaches the equilibrium solubility in each phase. Two fitting parameters were used: the local density of ferrite nuclei $N^{\alpha}_{\mathrm{loc}}$ and the local carbon concentration C_0 before the ferrite grain started to grow. The temperature T_{s} at which a ferrite grain started to grow is determined from the experimental growth curves and used as an input parameter for the model. Furthermore, the volume of the grains was calculated down to the temperature at which the start of the pearlite formation was experimentally observed (685 °C). The temperature dependence of the equilibrium concentrations of solute atoms in the parent phase and new phase is determined from the phase diagram. The equilibrium carbon concentrations in the austenite C^{γ}_{eq} and ferrite C^{α}_{eq} for the studied steel (see Section 3) are determined by MTDATA®. The dependence of the volume diffusion coefficient of carbon in austenite on the carbon concentration and the temperature that was determined by Ågren [24] is used in the calculations.

We assume that during the transformation the local density of ferrite nuclei $N^{\alpha}_{\mathrm{loc}}$ depends in the same way on time and temperature as the measured overall number of nuclei $N^{\alpha}_{\mathrm{norm}}$, normalized to the maximum value, which is shown in Fig. 4. The local density of ferrite nuclei can

Table 1
Parameters related to modeling the seven grains shown in Figs. 5 and 6

Grain no.	1	2	3	4	5	6	7
T_s (°C)	808.9	808.1	807.1	738.2	808.9	795.9	803.3
$N^{\alpha}_{loc,f} \times 10^{-13}$ (m^{-3})	1.5	3.5	3.6	7.5	0.65	3.7	1.9
C_0 (wt%)	0.235	0.260	0.265	0.540	0.200	0.260	0.279
$r_{c,s}$ (μm)	25	11	3.7	1.6	38	15	1.6

The temperature T_s at which a ferrite grain started to grow, the local density $N^{\alpha}_{loc,f}$ of ferrite grains at the end of the transformation, the local carbon concentration C_0 before the grain started to transform, and the position $r_{c,s}$ at which the diffusion profile starts to overlap for the first time are listed.

therefore be written as: $N^{\alpha}_{loc} = N^{\alpha}_{loc,f} N^{\alpha}_{norm}$, where $N^{\alpha}_{loc,f}$ is the local density of nuclei at the end of the transformation. In calculating the growth behavior of individual austenite and ferrite grains we included the measured ferrite fraction, shown in Fig. 3(a), in order to model the growth behavior of the average grain according to Eq. (4). The dotted line in Fig. 5 represents the Zener theory, which is only valid in the early stage of the transformation, for a grain that started to grow at the transition temperature of 822 °C in a region with a local carbon concentration that equals the overall composition of $C_0 = 0.214$ wt% carbon. The solid lines are fits with the model described in Section 2 to the measured growth curves. The fitting parameters of the individual grains shown in Figs. 5 and 6 are given in Table 1.

Fitting the model to ferrite grain No. 1 in Fig. 5(a) shows that the ferrite grain nucleated in a region with a slightly increased carbon concentration (0.235 wt%) with respect to the overall carbon concentration (0.214 wt%) of the alloy. The relatively low carbon concentration before the transformation and the relatively small number of neighboring nuclei result in two clearly separate growth stages during the transformation. Initially, the ferrite grain grows corresponds to the Zener theory described in Section 2.1, meaning that the diffusion fields do not overlap. At a later stage of the transformation the grain growth rate decreases, which corresponds to the overlap of diffusion fields, described in Section 2.2. The two growth stages of the ferrite can also clearly be observed in the decomposing austenite grains No. 5 and 6 in Figs. 6(a) and (b), respectively.

Fitting the model to ferrite grains No. 2 and 3 in Fig. 5(a) and (b) shows that the number of neighboring ferrite nuclei and the local carbon concentration before the transformation are approximately the same for both grains (see Table 1). The grains therefore reach approximately the same size (before the pearlite formation). Furthermore, the fitting parameters N^{α}_{loc} and C_0 are relatively high compared to grain No. 1 (see Table 1). As a result the diffusion field starts to overlap with neighboring grains much earlier than for grain No. 1. The fitting results of grains No. 4 and 7 show an even higher local carbon concentration before the ferrite grain started to grow. As can be seen from Table 1, these grains nucleated late and therefore are in a carbon rich environment. This results in a retarded growth in which the diffusion fields of neighboring ferrite grains almost immediately start to overlap after the ferrite grain nucleated. The position at which the diffusion profile of neighboring ferrite grains started to overlap for the first time for curves No. 4 and 7 is determined from the model as $r_{c,s} = 1.6$ μm.

Fitting the model to grain No. 5 in Fig. 6(a) shows that the ferrite grain nucleated in a region with a slightly decreased carbon concentration (0.200 wt%) with respect to the overall carbon concentration (0.214 wt%) of the alloy. This is likely the result of an inhomogeneous distribution of alloying elements (e.g. Mn, Cr, and Si) that attract or repel carbon atoms [23]. The reduced local carbon concentration combined with the low local density of ferrite nuclei results in a rapid decrease in austenite volume. The position at which the diffusion profile of the ferrite grain starts to overlap for the first time is therefore large ($r_{c,s} = 38$ μm).

A direct comparison between theory and experiment at the level of individual grains shows that the growth of ferrite grains depends strongly on the local carbon concentration and the local density of nuclei. Including these local conditions gives a much better description of the phase transformation kinetics of individual grains than models that are based on average grain growth behavior. Clearly, these deductions on the behavior of individual grains need further statistical support by analyzing more diffraction spots. Based on such a larger database the observed linear-like relationship between C_0 and the nucleation density (see Table 1) can be explored further and established more firmly. Supplementary experiments involving isothermal transformations on the same steel and linear cooling experiments on other steel grades are in progress and will lead to a further and better insight into the relationship between the local carbon composition and nucleation rate.

6. Conclusions

A simplified grain growth model is developed for solid-state transformations in polycrystalline materials

that involve solute partitioning and soft impingement. The model is in good agreement with the experimentally determined growth of individual ferrite grains in carbon steel.

The growth of ferrite grains depends strongly on the local carbon concentration and the local density of nuclei. Including these local conditions gives a much-refined description of the phase transformation kinetics than models that are based on average grain growth behavior. It is the strength of the 3DXRD-measurements in combination with this model, that the effect of the local composition on the transformation kinetics can now be probed. Furthermore, the experimental observation of decomposing individual austenite grains shows that there is carbon exchange between austenite grains during the transformation. For slow cooling conditions, per austenite grain approximately one ferrite grain nucleates. The austenite grain size is not stable prior to the transformation, probably due to coarsening effects.

Acknowledgements

This work was financially support in part by the Dutch Technology Foundation STW, Corus, SKF and Fundia Nedstaal. The ESRF is acknowledged for the provision of beam time. E.M.L., L.M., and H.F.P. acknowledge the support from the Danish National Research Foundation through the center Metal Structures in Four Dimensions, and the Danish Natural Sciences Research Council (via Dansync).

References

[1] Christian JW. The theory of transformations in metals and alloys. Oxford: Pergamon Press; 1981.
[2] Zackay VF, Aaronson HI, editors. Decomposition of austenite by diffusional processes. New York: Interscience; 1962.
[3] Mittemeijer EJ, Sommer F. Z Metallk 2002;93:352–61.
[4] Heckel RW, Paxton HW. Trans TMS-AIME 1960;218:799–806.
[5] Vandermeer RA. Acta Metall Mater 1990;38:2461–70.
[6] Van Leeuwen Y, Vooijs SI, Sietsma J, Van der Zwaag S. Metal Mater Trans A 1998;29:2925–31.
[7] Lauridsen EM, Jensen DJ, Poulsen HF, Lienert U. Scripta Mater 2000;43:561–3.
[8] Margulies L, Winther G, Poulsen HF. Science 2001;292:2392–934.
[9] Poulsen HF, Nielsen SF, Lauridsen EM, Schmidt S, Suter RM, Lienert U, et al. J Appl Crystallogr 2001;34:751–6.
[10] Offerman SE, Van Dijk NH, Sietsma J, Grigull S, Lauridsen EM, Margulies L, et al. Science 2002;298:1003–5.
[11] Zener C. J Appl Phys 1949;20:950–3.
[12] Wert C, Zener C. J Appl Phys 1950;21:5–8.
[13] Crespo D, Pradell T, Clavaguera-Mora MT, Claveguera N. Phys Rev B 1997;55:3435–44.
[14] Gilmour J, Purdy GR. Metall Trans 1972;3:3213–22.
[15] García de Andrés C, Capdevila C, Caballero FG, Bhadeshia HKDH. Scripta Mater 1998;39:853–9.
[16] Onink M, Brakman CM, Tichelaar FD, Mittemeijer EJ, Van der Zwaag S, Root JH, et al. Scripta Metall Mater 1993;29:1011–6.
[17] Te Velthuis SGE, Van Dijk NH, Rekveldt MTh, Sietsma J, Van der Zwaag S. Mater Sci Eng A 2000;277:218–28.
[18] Warren BE. X-ray diffraction. New York: Dover; 1990.
[19] Offerman SE, PhD thesis, Delft, Delft University Press, 2003.
[20] Offerman SE, Van Wilderen LJGW, Van Dijk NH, Sietsma J, Rekveldt MTh, Van der Zwaag S. Acta Mater 2003;51:3927–38.
[21] Thompson SW, Howell PR. Scripta Metall 1988;22:1775–8.
[22] Millitzer M, Pandi R, Hawbolt EB. Metall Mater Trans A 1996;27A:1547–53.
[23] Offerman SE, Van Dijk NH, Rekveldt MTh, Sietsma J, Van der Zwaag S. Mater Sci Technol 2002;18:297–303.
[24] Ågren J. Scripta Metall 1986;20:1507–10.